Pergamon

PII S1359-6454(96)00199-1

Acta mater. Vol. 45, No. 2, pp. 575–585, 1997

Published by Elsevier Science Ltd

1359-6454/97 $17.00 + 0.00

A TWO-DIMENSIONAL DIFFUSION MODEL FOR THE PREDICTION OF PHASE TRANSFORMATIONS: APPLICATION TO AUSTENITIZATION AND HOMOGENIZATION OF HYPOEUTECTOID Fe-C STEELS

A. JACOT† and M. RAPPAZ

Laboratoire de Métallurgie Physique, Ecole Polytechnique Fédérale de Lausanne, MX-G, CH-1015 Lausanne, Switzerland

(Received 25 January 1996; accepted 23 May 1996)

Abstract—A two-dimensional (2D) model has been developed for the prediction of diffusive phase transformations (e.g. α to γ). For that purpose, the diffusion equations are solved within each phase (α and γ) using an explicit finite volume technique formulated for a regular hexagonal grid. The discrete α/γ interface is represented by special volume elements α/γ. An α volume element undergoes a transition to an α/γ interface state before becoming γ. This procedure allows us to handle the displacement of the interface while respecting the flux condition at the interface. The model has been applied to the austenitization of a hypoeutectoid plain carbon steel during heating. Simulated microstructures showing the dissolution of ferrite particles in the austenite matrix are presented at different stages of the phase transformation. Specifically, the influence of the microstructure scale and of the heating rate on the transformation kinetics has been investigated. Reverse TTT-diagrams calculated with this 2D model are compared with experimental results from the literature and with the predictions of a simpler one-dimensional (1D) front-tracking calculation. Finally, it is shown that interface instabilities leading to the formation of dendrites can also be reproduced by such a model. *Copyright © 1997 Acta Metallurgica Inc.*

1. INTRODUCTION

The modelling of microstructure formation in materials processing has progressed markedly over recent years, especially in the fields of recrystallized structures [1–4], of grain structure formation in solidification processes [5, 6] and of dendritic growth [7]. Modelling provides images that reproduce actual microstructures. It has also become increasingly important in predicting microstructural defects and final mechanical properties. However the complexity of the solid-state transformations and the presence of multiple phases and morphologies has limited the use of these techniques in the field of heat treatment of steels. The first step in modelling the heat treatment of steels is to consider the phase transformations occurring upon heating, because the state of the microstructure after heating (volume fraction, concentration homogeneity and density of the austenite grains) has a great influence upon the kinetics of the phase transformation during cooling and on the subsequent mechanical properties of the steel. Most of the models predicting the kinetics of microstructure formation during austenitization of steels are based upon experimental TTT diagrams and some kind of additivity principle [8–10]. Such principles allow the data obtained under isothermal conditions to be applied to the calculation of transformation kinetics during continuous heating. Nevertheless, such models are quite limited in their applications, because the experimental data only apply for a given initial microstructure.

An alternative approach to the prediction of diffusive phase transformations is to solve the diffusion equation in a representative domain of the microstructure where the evolving phases (ferrite, cementite and austenite) are described. This has been achieved in one dimension (1D) for the prediction of homogenization times [11] and reverse TTT-diagrams [12]. Some attempts have also been made in two dimensions (2D) for the calculation of microstructures [13, 14]. However, such 2D models have not explicitly accounted for the boundary conditions at the moving interface. It is well established that two conditions must be imposed at the interface. One is dictated by the equilibrium phase diagram, and the second is the solute flux balance.

The present paper describes a general two-phase model for the prediction of microstructural evolution in a material which undergoes a diffusive phase transformation α to γ. The diffusion equations in the α and γ phases are solved in 2D using an explicit finite volume scheme. The boundary conditions at the α/γ boundary are accounted for using special interface elements. The flux condition at the interface is replaced by a phase-field evolution (in this case, the

†To whom all correspondence should be addressed.

volume fraction of α) spread over one mesh size. The model has been applied to the austenitization of hypoeutectoid steels during heating. The results of the model are compared with those obtained from a front-tracking 1D model and with experimental results extracted from the literature. In addition, this 2D approach is shown to be generally applicable by reproducing dendrite formation during solidification as a result of interface instabilities.

2. MODELLING

Assuming that the α/γ transformation is only governed by solute diffusion, the kinetics can be described by the following diffusion equations:

$$\frac{\partial c_v}{\partial t} = \text{div}\, D_v(c_v, T)\, \mathbf{grad}\, c_v \quad \text{in } \Omega_v = \Omega_\alpha \text{ or } \Omega_\gamma \quad (1)$$

$$D_\gamma \left[\frac{\partial c_\gamma}{\partial n}\right]^* - D_\alpha \left[\frac{\partial c_\alpha}{\partial n}\right]^* = v_n(c_\alpha^* - c_\gamma^*) \text{ at } \partial\Omega_{\alpha/\gamma} \quad (2)$$

t is the time, c_v is the carbon concentration in the phase v (α or γ) and D_v the associated diffusion coefficient, v_n is the normal velocity of the α/γ interface $\partial\Omega_{\alpha/\gamma}$ (i.e. $v_n = \mathbf{v}\cdot\mathbf{n}$), $\mathbf{n}$ is the normal to this interface pointing outwards, Ω_α, c_α^* and c_γ^* are the concentrations at the interface in the α and γ domains, respectively. The symbol * denotes values taken at the interface whereas $\partial/\partial n$ is the normal derivative (i.e. $\partial c/\partial n = \mathbf{grad} c \cdot \mathbf{n}$). The boundary condition set for the external boundary of the domain $\Omega = \Omega_\alpha \cup \Omega_\gamma$ is that of a closed system, whereas the initial condition for the concentrations in each domain is given by:

$$c_v(\mathbf{x}, t = 0) = c_v^*(T_i) \quad (3)$$

where $c_v^*(T_i)$ is the concentration at the initial temperature T_i. It is given by the phase diagram

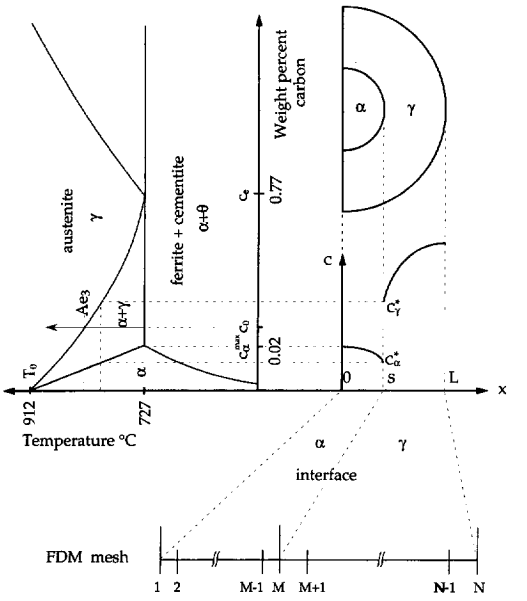

Fig. 1. Representation of the 1D domain [0, L] (spherical geometry), of the solute profiles in the α and γ regions and of the corresponding equilibrium phase diagram.

assuming equilibrium. Notice that the diffusion coefficient in each phase, D_v, can be concentration- and temperature-dependent. The temperature history of the specimen, $T(t)$, is a given function of time and is considered to be uniform in the calculation domain. This can be justified by the fact that thermal diffusion is much faster than diffusion of solute atoms.

This well-posed diffusion problem has been solved for both 1D and 2D. The results of the 1D solution are used to validate the 2D algorithm.

2.1. 1D model

In the 1D model, a "typical" volume element of the microstructure composed of both phases α and γ is

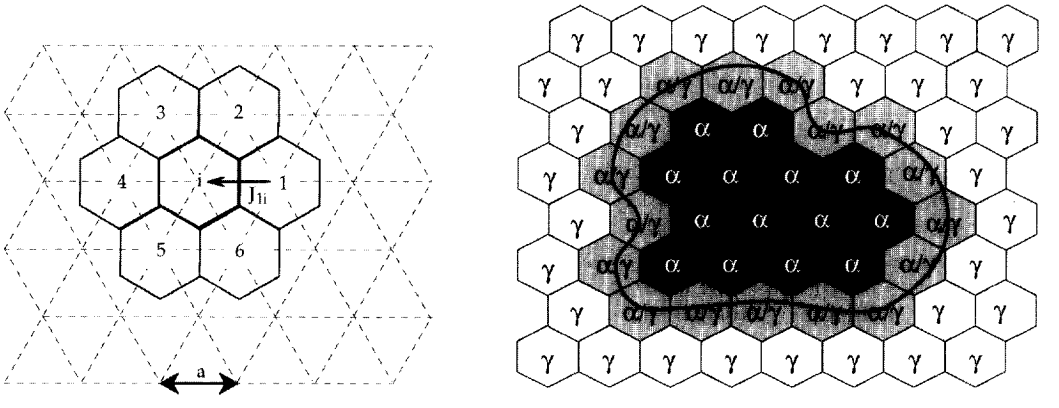

a b

Fig. 2. Illustration of the hexagonal grid used to solve the solute diffusion equations in 2D. The arrow represents the flux J_{1i} going from neighbour 1 to the central cell i. The right part illustrates the layer of interface cells which separate the α and γ domains.

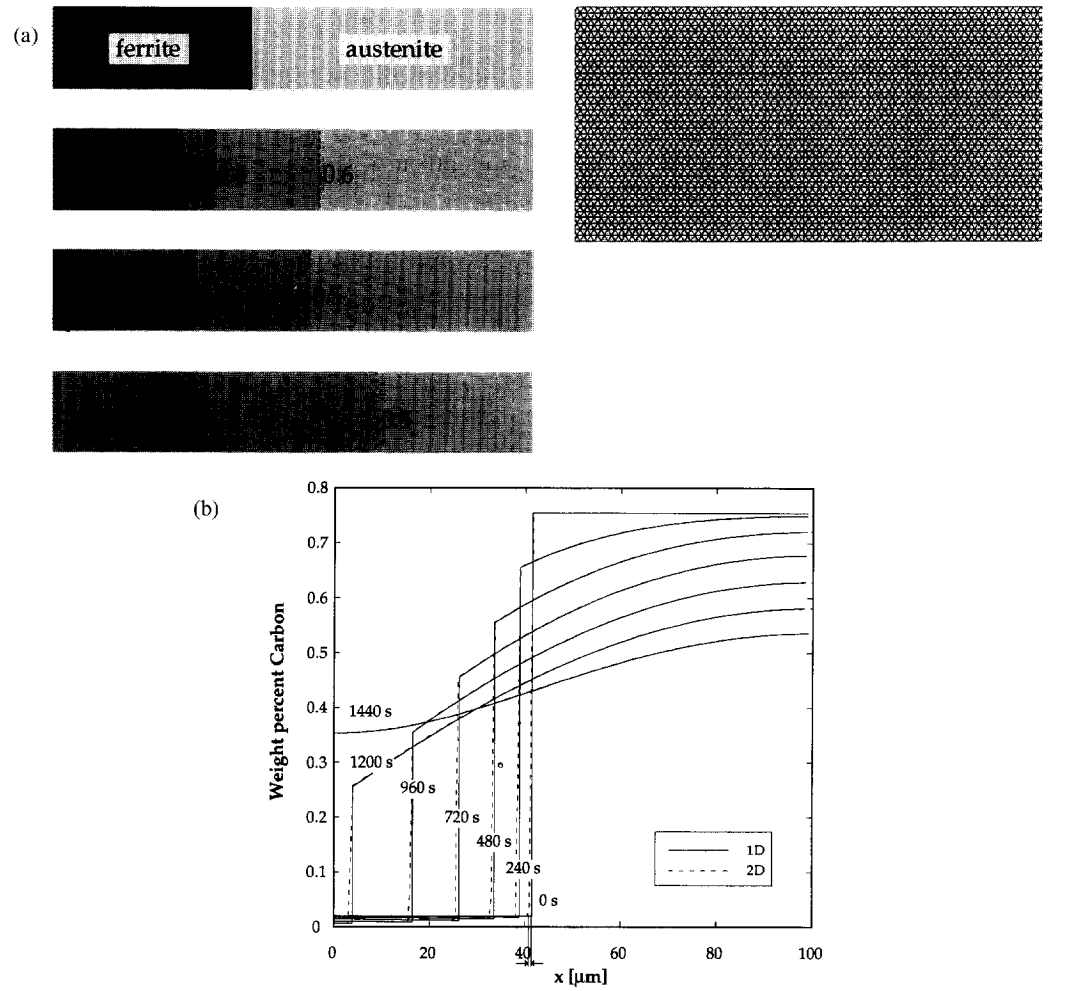

Fig. 3. (a) Concentration fields at four different times (0, 720, 1200 and 1400 s) as predicted by the 2D model using the 100 × 500 hexagonal grid shown on the right. The values indicate the carbon concentration of the vertical isopleths (dotted lines). The plain line represents the α/γ interface. (b) Comparison of the concentration profiles predicted by the 1D model (continuous lines) and the 2D model (dotted lines). Heating rate 0.1°C/s, nominal carbon concentration of the alloy 0.49 wt%.

considered. In Fig. 1, the top right illustration shows these two domains for a spherical (or cylindrical) geometry. However, the model can also be applied to cartesian geometries. This initial volume fraction of α is given by the lever rule:

$$f_\alpha = \frac{c_\gamma(T_i) - c_0}{c_\gamma(T_i) - c_\alpha(T_i)} \tag{4}$$

where c_0 is the nominal concentration of the alloy and $c_\alpha(T_i)$ and $c_\gamma(T_i)$ are the concentrations in both phases given by the phase diagram for the temperature T_i. Using x for the space variable and $s(t)$ for the position of the α/γ interface (see Fig. 1), equations (1) and (2) can be written as:

$$\frac{\partial c_v}{\partial t} = \frac{1}{x^m}\frac{\partial}{\partial x}\left(x^m D_v \frac{\partial c_v}{\partial x}\right) \quad v = \begin{cases}\alpha \text{ for } x \in [0, s(t)] \\ \gamma \text{ for } x \in [s(t), L]\end{cases} \tag{5}$$

$$v(c_\alpha^* - c_\gamma^*) = D_\gamma\left(\frac{\partial c_\gamma}{\partial x}\right)^* - D_\alpha\left(\frac{\partial c_\alpha}{\partial x}\right)^* \text{ for } x = s(t). \tag{6}$$

The geometrical parameter m is equal to 0, 1 or 2 for the planar, cylindrical and spherical geometries, respectively. The boundary conditions at the external boundary of the domain and the initial conditions are given by:

$$\frac{\partial c_v}{\partial x} = 0 \quad x = 0, L \tag{7}$$

$$c(x,0) = \begin{cases}c_\alpha(T_i) \text{ for } x \in [0, s(t)] \\ c_\gamma(T_i) \text{ for } x \in [s(t), L]\end{cases} \tag{8}$$

Equations (5–8) have been solved using a finite differences method and a procedure which follows the movement of the α/γ interface. The details are given in the Appendix.

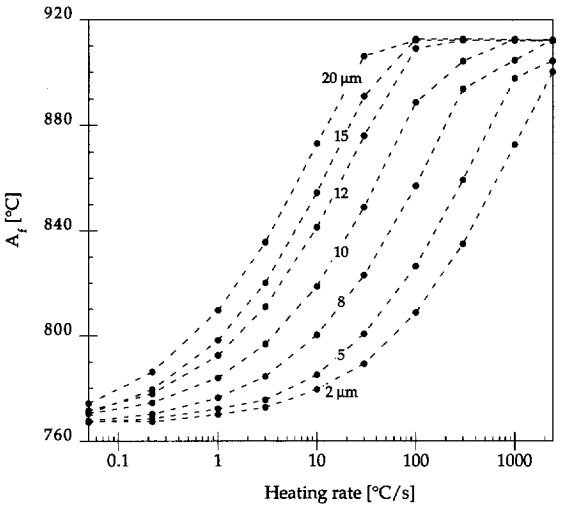

Fig. 4. Final austenitization temperature, A_t, as a function of the heating rate as calculated for a Fe-0.49 wt% C steel using the 1D model. The various curves correspond to different sizes of the calculation domain.

2.2. 2D Model

Modelling the two-phase diffusion in two dimensions is much more complex than the 1D equivalent, because the geometry of the interface must be solved together with the diffusion equation. Such a problem may lead to instabilities of the interface (formation of cells or dendrites). In such cases, interfacial energy, interfacial energy anisotropy and elastic energy of coherent interfaces play important roles in controlling the interface morphology. Austenitization of normalized hypoeutectoid steels proceeds with stable α/γ boundaries, and the interfacial energy contribution can be neglected. This assumption has been made in the model presented here.

The problem is solved using a regular hexagonal grid (see Fig. 2(a)). A hexagonal volume element (or cell) is attributed to each nodal point and can take three different states: α, γ or "interface". A layer of interface cells always separates γ from α volume elements, which are not allowed to be adjacent (see Fig. 2(b)). The solute concentration in each of these cells is given by c_i, where i is the cell index. The interface cells are characterized by three additional variables: $c_i^{\alpha *}$ and $c_i^{\gamma *}$, the solute concentrations at the interface in the α and the γ phases, respectively, and f_i^{α}, the volume fraction of phase α. Since local equilibrium is assumed at the α/γ interface, $c_i^{\alpha *}$ and $c_i^{\gamma *}$ are given by the phase diagram, whereas the volume fraction f_i^{α} is calculated from the lever rule:

$$f_i^{\alpha} = \frac{c_i^{\gamma *} - c_i}{c_i^{\gamma *} - c_i^{\alpha *}}, \tag{9}$$

†Although k refers to a local numbering of the neighbouring cells ($k = 1, 6$) and not to their global number, it will be kept for the sake of simplicity instead of an index $j(k)$.

where c_i is the concentration in the interface cell.

The solute diffusion between the cells is described using an explicit finite volume approach. A mass balance is achieved for each cell i according to the concentration of the six neighbouring cells:

$$V \frac{\Delta c_i}{\Delta t} = \sum_{k=1}^{6} S J_{ki} \tag{10}$$

with

$$V = \frac{\sqrt{3}}{2} a^2 \text{ and } S = \frac{a}{\sqrt{3}} \tag{11}$$

where a is the lattice parameter of the hexagonal network of cells, V and S are the surface and the edge length of the cells, Δt is the time step, Δc_i is the variation of carbon concentration in cell i and J_{ki} is the flux of solute atoms from the kth neighbouring cell to the central cell i ($k = 1, 6$)†. This solute flux is calculated according to the state of the neighbouring cells.

(a) The cells k and i belong to the same phase v (α or γ),

$$J_{ki} = D_v(\bar{c}, T) \frac{c_k - c_i}{a} \text{ with } \bar{c} = \frac{c_k + c_i}{2}. \tag{12}$$

(b) The cell i belongs to phase v whereas cell k belongs to the interface:

$$J_{ki} = D_v(\bar{c}, T) \frac{c_k^{v *} - c_i}{a} \text{ with } \bar{c} = \frac{c_k^{v *} + c_i}{2}. \tag{13}$$

(c) Both cells belong to the interface:

$$J_{ki} - \bar{f}_{\alpha} D_{\alpha}(\bar{c}_{\alpha}, T) \frac{c_k^{\alpha *} - c_i^{\alpha *}}{a} + (1 - \bar{f}_{\alpha}) D_{\gamma}(\bar{c}_{\gamma}, T) \frac{c_k^{\gamma *} - c_i^{\gamma *}}{a}$$

with

$$\bar{c}_{\gamma} = \frac{c_k^{\gamma *} + c_i^{\gamma *}}{2}, \; \bar{c}_{\alpha} = \frac{c_k^{\alpha *} + c_i^{\alpha *}}{2} \text{ and } \bar{f}_{\alpha} = \frac{f_i^{\alpha} + f_k^{\alpha}}{2}. \tag{14}$$

In order to avoid border effects, periodic boundary conditions are applied to the cells located near the edges (e.g. the cells located on the right boundary of the domain are the left neighbours of the cells located on the left boundary). The time step, Δt, is given by the stability criterion of the explicit scheme: it is calculated for the maximum tabulated value of the diffusion coefficient, $D_{\max}$, and is given by:

$$\Delta t < \frac{a^2}{4 D_{\max}} \tag{15}$$

as would be for a regular cartesian mesh. At each time step, the new carbon concentration of the interface cells is converted into a new phase fraction using equation (9). If f_i^{α} falls below zero during heating, the interface cell is attributed to γ. All the α neighbour cells which are adjacent to this cell are

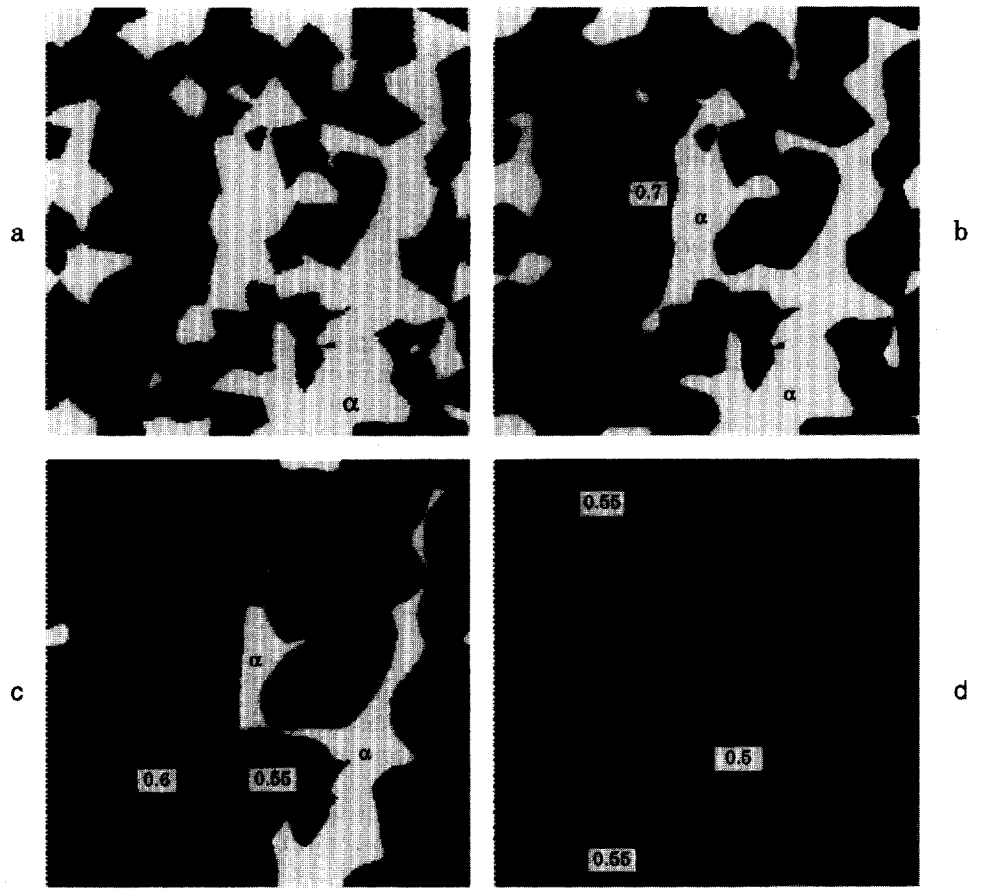

Fig. 5. Evolution of the microstructure during the austenitization process as calculated with the 2D model for a heating rate of 10°C/s. The microstructure is shown at 0, 2.5, 5 and 8 s, the white zones representing ferrite regions which are progressively dissolved in the austenitic matrix (in dark). The values indicate the carbon concentration of the isopleth lines. (12.5 μm × 12.5 μm hexagonal mesh, 40 000 cells.)

changed to interface cells so that α and γ cells are never adjacent.

3. AUSTENITIZATION OF NORMALIZED HYPOEUTECTOID CARBON STEELS

The mechanisms and the kinetics of the austenitization process in normalized hypoeutectoid carbon steels have been widely discussed in the literature [15–17]. It appears that the transformation may be considered to occur in two steps: the pearlite dissolution and then the transformation of proeutectoid ferrite into austenite. The first step occurs above the eutectoid temperature and is governed by the dissolution kinetics of cementite and by the carbon diffusion in the lamellae of ferrite. It is relatively rapid since the diffusion distances are short. The second step occurs within a temperature range which is limited by the eutectoid line and the α/γ transition temperature of pure iron‡. The maximal amount of austenite that can form at any temperature is given by the phase diagram and the lever rule: it reaches 100% at Ae3 (the $(\alpha + \gamma)/\gamma$ line of the equilibrium phase diagram). The kinetics of transformation are dictated by the diffusion of carbon atoms from the solute-rich austenite regions (coming from previously pearlitic zones) to the proeutectoid ferrite grains. Therefore, the solute flux balance at the ferrite/austenite interface must be considered.

The kinetics of the austenitization process is thus mainly controlled by the second stage of the transformation, i.e. by the transformation of α grains through the diffusion of carbon. In the models presented here, it has been assumed that the time required for the dissolution of pearlitic lamellae is negligible in comparison with the duration of the second reaction. Accordingly, the microstructure at the end of the first stage (austenite regions and ferrite grains) is used as the initial state for the model. The amount of austenite corresponding to former pearlitic regions is calculated using the lever rule and the nominal concentration of the alloy.

‡This limit temperature of 912°C is based upon the assumption of an α/γ interface at equilibrium.

4. APPLICATION OF THE MODEL TO THE AUSTENITIZATION OF HYPOEUTECTOID STEELS

4.1. Validation of the 2D algorithm

The 2D model was first applied to a 1D problem in order to compare the results with the front-tracking 1D model. A rectangular domain was initially subdivided into two zones (ferritic and austenitic) according to a vertical planar interface. Taking the start of the austenitization process at the eutectoid temperature and assuming equilibrium, the initial carbon concentration was set to 0.8 wt% (eutectoid composition) in the austenite and to 0.02 wt% in the ferrite (c_α^{max}, see Fig. 1). The initial volumetric phase fraction of ferrite was determined from the nominal composition of the alloy (0.49 wt%) using the lever rule (equation (4)). The temperature of the domain was then increased at a constant rate of 0.1°C/s. Assuming local equilibrium at the α/γ interface, the thermal history and the phase diagram directly give the carbon concentration $c_\alpha{}^*(t)$ and $c_\gamma{}^*(t)$ of the interfacial cells.

Figure 3(a) shows the concentration fields in the domain at four different times together with the hexagonal mesh used for the computations. The vertical lines and associated values are the carbon isopleth lines in the austenite region. As can be seen, the interface remains stable and planar during the entire transformation process. Concentration profiles are compared with profiles obtained with the 1D model in Fig. 3(b) at seven different instants (from 0 to 1440 s). As expected, the agreement is excellent. The only difference that can be observed is for the concentration jump at the interface. It is spread over one layer of the mesh in the 2D model, whereas it is a sharp transition in the case of the front-tracking 1D model. It can be concluded that the 2D model correctly predicts the kinetics of the phase transformation and does not introduce interface instabilities in this particular case. Moreover, the numerical diffusion at the interface is limited to one layer thickness.

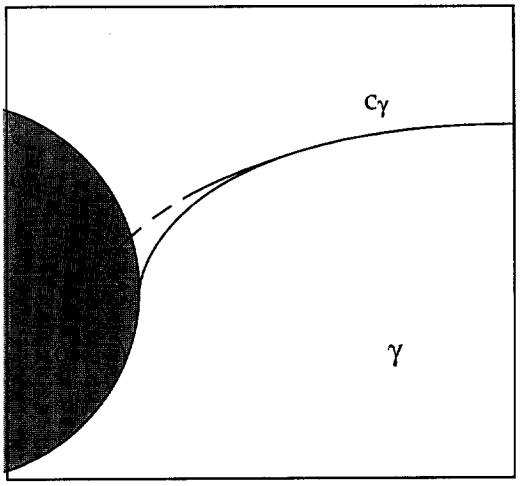

Fig. 6. Schematic diagram showing the perturbation of the interface of a ferrite grain which is dissolved in a matrix of austenite. A local increase of the interface velocity during heating (concave perturbation of the α grain) induces a decrease of the concentration gradient in the γ phase and thus slows down the interface (i.e. stable interface).

4.2. 1D computation of reverse TTT diagrams

The 1D spherical model has been applied to the prediction of the austenitization kinetics of a 0.49 wt% carbon steel using various heating rates (0.05, 0.22, 1, 3, 10, 30, 100, 300, 1200, 2400°C/s). The initial conditions were determined according to the procedure described in the previous section. In order to predict more realistically the transformation kinetics, the temperature- and concentration-dependencies of the diffusion coefficient of carbon in austenite were accounted for according to Badeshia's approach [18]. The diffusion coefficient of carbon in ferrite was assumed to depend only on the temperature. The following expression was used [19]:

$$D_\alpha(T) = D_{0\alpha}\exp(-Q_\alpha/RT) \text{ with}$$

$$D_{0\alpha} = 2 \times 10^{-6}\ \text{m}^2/\text{s and } Q_\alpha = -84100\ \text{J/mole}. \quad (16)$$

Calculations were performed with a regular mesh of 1000 nodes and a variable domain size (from 2 to 20 μm).

The temperature corresponding to complete transformation of the α to γ, A_f, has been plotted as a function of the heating rate in Fig. 4, which is referred to as a reverse TTT diagram. It can be observed that A_f is limited by two extreme values. At very low heating rate (0.05°C/s), the carbon concentration remains uniform in both phases during the transformation and the austenitization ends just above A_{e3} (770°C, see Fig. 1). At high heating rate, the transformation ends at 912°C, the transition temperature from α to γ of pure iron (the temperature T_0 in the phase diagram of Fig. 1). Since both $c_\alpha{}^*$ and $c_\gamma{}^*$ vanish near this temperature, this allows the interface velocity to increase up to very high values and the transformation to be completed extremely rapidly. However, the local equilibrium assumption is probably no longer valid in such a situation, because the attachment kinetics of atoms at the interface becomes important. Therefore, this calculation should only be considered as a lower limit for A_f.

In order to investigate the effect of the initial microstructure on the transformation kinetics, the computations have been repeated using several domain sizes, L, ranging from 2 to 20 μm. The resulting reverse TTT diagrams have also been drawn in Fig. 4. It can be observed that the initial size of the ferritic domains has a strong influence on the transformation kinetics. For example, changing the ferritic zones from 2 μm to 20 μm increases A_f from 775°C to 870°C for a heating rate of 10°C/s. For an initial eutectoid temperature equal to 725°C, the temperature interval of the completed transformation is increased by a factor of three (50°C for the finest

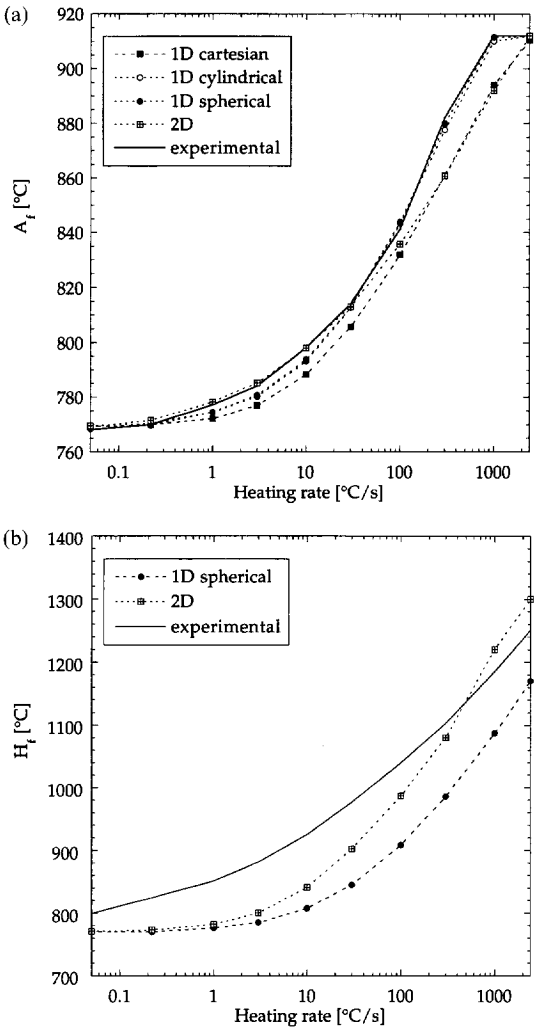

Fig. 7. Final austenitization temperature, A_f (a) and homogenization temperature, H_f, (b) as a function of the heating rate as calculated for a Fe-0.49 wt% C steel. The results of the 1D model have been obtained for a 4 μm domain assuming cartesian, cylindrical or spherical geometry. The results of the 2D model have been obtained with the initial microstructure shown in Fig. 5(a) (12.5 μm × 12.5 μm hexagonal mesh of 10 000 cells). These calculated curves are compared with the experimental result [20].

microstructure compared to 145°C for the coarsest one). This illustrates the importance of the initial microstructure for the modelling of the phase transformation kinetics. It also demonstrates the utility of simulation for complementing the sparse experimental data that are usually available in the field of transformation kinetics.

4.3. 2D calculations

The first step of a 2D calculation is the production of a realistic initial microstructure. This was achieved numerically according to the following procedure. Ferrite and pearlite spherical grains were grown from randomly located nucleation sites until the calculation domain was totally filled. The nuclei were randomly attributed to ferrite or pearlite with a probability given by the desired phase fraction. The nucleation centre of a given grain was located in a cell j of the enmeshment used for the diffusion calculation. The time t_j^i at which this grain could capture another cell i was given by:

$$t_j^i = \tau_j + d_{ij}/v \tag{17}$$

where v is a constant growth rate, τ_j is the nucleation time of grain j and d_{ij} is the distance separating the cells i and j. Considering all the nucleated grains, a cell i will be effectively captured by the grain k given by the smallest t_j^i value, i.e. $t_k^i = \min_j \{t_j^i\}$. The phase the grain k belongs to is of course attributed to the captured cell i. In order to account for the periodic boundary conditions, each nucleated grain was duplicated in the eight rectangles surrounding the calculation domain. The result of the initialization procedure is shown in Fig. 5(a) for 0.49 wt% carbon steel. This 12.5 μm × 12.5 μm microstructure was generated using a grain density of 1×10^{12} nuclei/m^2. The light zones represent the ferritic phase (41% of the surface) while the dark matrix corresponds to austenite (previously assumed to be the pearlite grains).

The 2D calculations were performed using a 100 × 116 mesh with a parameter $a = 0.5$ μm and a time step of 10^{-3} s. The result of a simulation obtained with a constant heating rate of 10°C/s is shown in Fig. 5. The concentration field in the microstructure is represented at four different times ($t = 0$, 2.5, 5 and 8 s) with different grey levels. Figure 5(d) shows that the specimen is totally austenitic after 8 s and that the carbon concentration is nearly homogeneous (between 0.5 and 0.55 wt%). During the transformation process, it can be seen that the ferrite grains shrink but keep their shape. The corners of the grains become smooth, because diffusion occurs more rapidly in these regions. There is no evidence of interface instabilities. It should be emphasized that the application of the model did not produce any unstable interface, even at the highest heating rate. The situation, which is similar to the last solidification of liquid droplets, appears to be physically stable, as schematically shown in Fig. 6. If a small perturbation developed at the α/γ interface (e.g. local concavity of the α particle), the flux of carbon flowing from the γ matrix would be reduced. This would also slow down the velocity of the α/γ interface and thus tend to eliminate this perturbation.

4.4. 2D computation of reverse TTT diagram

Similar 2D calculations have been performed using various heating rates (0.05, 0.22, 1, 3, 10, 30, 100, 300, 1200, 2400°C/s) in order to construct a reverse TTT diagram. The result shown in Fig. 7(a) can be compared with simulated curves obtained with the 1D model and with an experimental curve for a Ck45 steel taken from [20]. The 1D calculations were

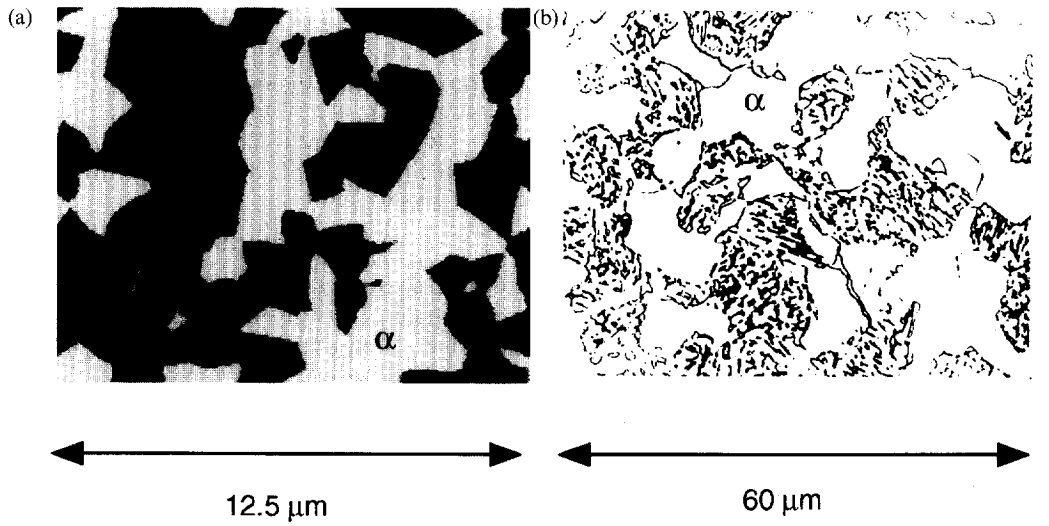

Fig. 8. Initial microstructures of a Fe-0.49 wt% C steel used for the 2D computations of Fig. 5(a) and taken from Ref. [20] (b).

performed using a 4 μm domain size and for the cartesian, cylindrical and spherical geometries. The predicted curves are almost superimposed for the spherical and cylindrical cases while small differences can be observed for the cartesian geometry. This means that a cylinder of ferrite transforms at about the same rate, df_α/dt, as a spherical particle having the same initial volume fraction of α. This observation suggests that 2D simulations might be adequate instead of more time-consuming 3D calculations.

As can be seen in Fig. 7(a), the 1D and 2D models reproduce the shape of the experimental curve quite well. This good agreement was achieved using the initial microstructure shown in Fig. 8(a). As can be seen, this microstructure is much finer than that observed in the sample used to measure the experimental curves [20] (Fig. 8(b)): the appearance of the ferrite and pearlite regions is about the same in both figures but there is about a factor 5 in the scale! This means that the model predicts transformation kinetics which are too slow with respect to the experiment. This result is somewhat surprising because one can envisage various mechanisms which have not been considered in the simulation and which would make the calculated transformation kinetics even slower: the attachment kinetics of atoms at the interface, or the time required to nucleate austenite and to transform pearlite. The faster transformation rate observed experimentally might be explained by the presence of some alloying elements like Mn (0.74%) and Cr (0.16%). Such substitutional atoms induce a deformation of the f.c.c. lattice which increases the diffusivity of interstitial atoms. Another mechanism could be the diffusion at grain boundaries which would enhance the rate of the transformation.

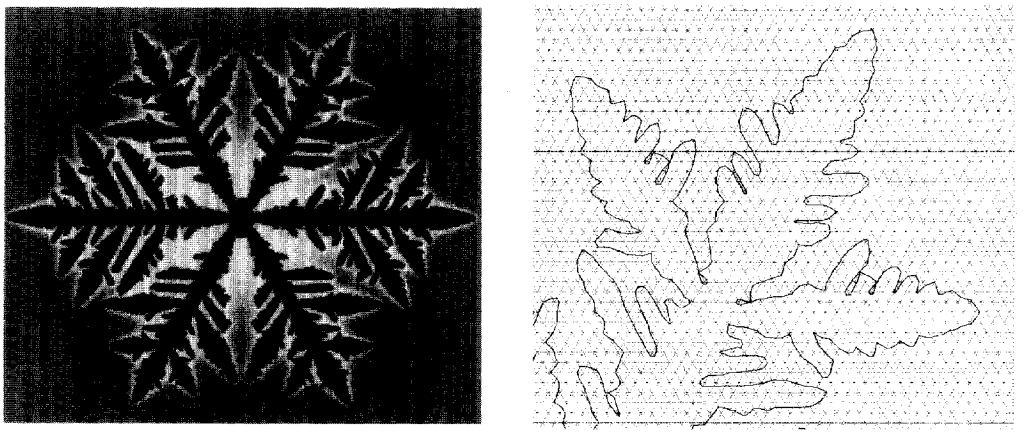

Fig. 9. Equiaxed dendrite predicted from the 2D diffusion calculation using isothermal conditions (0.5°C undercooling). The physical properties of the succinonitrile-1.3% acetone alloy (liquidus slope equals −2.8 K/wt%, partition coefficient equals 0.1) have been used. The enlargement shows the tip of the dendrite superimposed with the hexagonal mesh (150 μm × 150 μm mesh of 40 000 cells).

4.5. Homogenization

The diffusion model was used to describe the homogenization of the carbon concentration that takes place in the austenite after the completion of the phase transformations. The homogenization of austenite is very important for the quenching of steels since the local carbon concentration dictates the microhardness of the martensite in the final structure. The prediction of the homogenization temperature, H_f, requires the definition of a criterion. In the present investigation, the sample was considered to be homogeneous when the difference between the maximal and minimal carbon concentrations was smaller than 0.5% of the nominal composition. Figure 7(b) compares the results obtained for continuous heating with the 1D and 2D models with an experimental curve taken from [20]. The temperature, H_f, at which the sample is homogeneous has been plotted as a function of the heating rate. The temperatures predicted with the 2D model are somewhat higher than those obtained with the 1D model. This result occurs because some very large ferrite or pearlite grains may be present in the initial 2D microstructure. Thus, the homogenization can take a longer time to complete than for the 1D model, which assumes an average grain size. At very low heating rates, the carbon concentration remains uniform in both phases during the transformation and the sample is already homogeneous when the ferrite is dissolved. In this case, similar results are obtained with the 1D and 2D models. It can be observed that the experimental temperatures, H_f, measured at a low heating rate are higher than those obtained from the simulation. The criterion for homogenization, however, is not well defined in the experiments of [20], and other alloying elements might also affect the results by increasing the rate of diffusion.

5. APPLICATION TO OTHER DIFFUSIVE PHASE TRANSFORMATIONS

An attempt has been made to apply the model to the solidification of a melt from a small spherical solid nucleus. The undercooling was assumed to be constant (i.e. isothermal solidification). Some experimental data relevant to this case are given in the figure caption. As illustrated in Fig. 9(a), the calculation in this case reflects the unstable nature of the solid–liquid interface and generates an equiaxed dendrite. The grey levels shown in this figure correspond to the solute concentration: because the partition coefficient k is smaller than unity, the solid dendrite has the smallest concentration. (It is uniform since there is no curvature contribution and the undercooling is constant.) The grey background corresponds to the nominal concentration of this alloy and the white regions near the dendrite interface are the solute-rich liquid zones. Since there is no stabilizing curvature term, the geometry and the spacing of the dendrite arms are dictated by the six-fold symmetry of the mesh and the size of the volume elements. The enlargement of one of the tips of the dendrite shown in Fig. 9(b) clearly shows that its radius of curvature is of the same order of magnitude as the mesh size. The isoline outlining the dendrite shape corresponds to a volume fraction of solid $f_s = 0.5$ (i.e. the interface cells are precisely located on the dendrite contour). Algorithms accounting for the curvature of the interface are being developed in order to produce more realistic dendrites. If successful, such a method could be an alternative to the phase-field technique [7] since the diffuse interface in this case is only spread over one mesh size.

6. CONCLUSIONS

A numerical model has been developed in order to calculate the solute diffusion in a two-dimensional and two-phase domain, using special interfacial elements. The solute flux condition at this moving boundary and the equilibrium condition were calculated. This 2D model has been applied to the austenitization of hypoeutectoid carbon steels during continuous heating. Compared with similar 1D models, this technique offers several advantages: realistic microstructures with a wide distribution of particle size and morphology, the use of a digitized micrographs as a starting microstructure, and more realistic output of microstructures during the transformation process in the form of 2D-images.

Some differences between calculated and experimental transformation kinetics have been noticed. In particular, it has been shown that reverse TTT diagrams can be described accurately by the diffusion models, providing the size of the microstructure is refined compared with experiment. Without changing the microstructure scale, the diffusion coefficient would have to be multiplied by a factor of 25 in order to obtain agreement with the experiment. This discrepancy requires additional investigation. A possible explanation might be that additional alloying elements enhance the diffusion of carbon. Another explanation might be enhanced diffusion at grain boundaries. These two mechanisms could be accounted for in the 2D model without too many difficulties.

It has been shown that the same 2D model can be used to simulate other diffusive phase transformations. A simulation of equiaxed solidification was attempted. Instability of the interface was demonstrated but it appears that it is necessary to introduce curvature effects if realistic morphologies and growth kinetics are to be simulated. Such developments are under way and could possibly be an alternative to the phase-field method [7].

Finally, the choice of a hexagonal grid to solve the diffusion equation has been dictated by the fact that this model will be ultimately coupled with a

Monte-Carlo simulation of the austenite grain growth [1]. This will provide a comprehensive model for the predictions of the different mechanisms that are observed during the austenitization process: formation of austenite, homogenization and grain growth.

Acknowledgements—The financial support of the Commission pour l'Encouragement de la Recherche Scientifique, Bern, (CERS Grant 2568.2) and of the companies Amysa-Yverdon SA, Yverdon, Bobst SA, Prilly, and Calcom SA, Lausanne, is greatly acknowledged.

REFERENCES

1. D. J. Srolovitz, M. P. Anderson, G. S. Grest and P. S. Sahni, *Acta metall.*, **32,** 783 (1984); *Acta metall.* **32,** 793 (1984); *Acta metall.* **32,** 1429 (1984); *Acta metall.* **33,** 509 (1985); *Acta metall.* **33,** 2233 (1985).
2. H. V. Atkinson, *Acta metall.* **36,** 469 (1988).
3. S. Ling and M. P. Anderson, *JOM*, Sept (1992).
4. A. D. Rollet, D. J. Srolovitz and M. P. Anderson, *Acta metall.*, **37,** 1227 (1989).
5. M. Rappaz, *Int. Mat. Reviews*, **34,** 93 (1989).
6. Ch.-A. Gandin and M. Rappaz, *Acta metall. mater.*, **42,** 2233 (1994).
7. J. Warren and W. J. Boettinger, *Acta metall. mater.*, **43,** 689 (1995).
8. J. B. Leblond and J. Devaux, *Acta metall.*, **32,** 137 (1984).
9. S. Denis, D. Farias and A. Simon, *ISIJ Int.*, **32,** 316 (1992).
10. T. T. Pham, E. B. Hawbolt and J. K. Brimacombe, *Met. Trans.*, **26A,** 1987 (1995).
11. B. Karlsson and L.-E. Larsson, *Mat. Sci. and Eng.*, **20,** 161 (1975).
12. T. Akbay, R. C. Reed and C. Atkinson, *Acta Met.*, **47,** 1469 (1994).
13. K. Inoue, E. Ohmura, K. Haruta and S. Ikuta, *Trans of JWRI*, **16,** 49 (1987).
14. K. Inoue, E. Ohmura and S. Ikuta, *Trans of JWRI*, **16,** 97 (1987).
15. G. A. Roberts and R. F. Mehl, *Trans. ASM*, **31,** 613 (1943).
16. B. Karlsson, *Z. Metallkunde*, **63,** 161 (1972).
17. D. Farias, Ph.D. Thesis, I.N.P.L., Nancy, (1991).
18. H.K.D.H. Badeshia, *Metal Science*, **15,** 477 (1981).
19. C. Wert, *Phys. Rev.* **79,** 601 (1950).
20. *Atlas zur Wärmebehandlung der Stähle*, Verlag Stahleise GmbH, Düsseldorf (1954).

APPENDIX

The FDM solution of the 1D problem follows a procedure similar to that given in [11]. A uniform mesh of M nodes is defined for the α region ($0 \leqslant x \leqslant s(t)$), whereas the γ region ($s(t) \leqslant x \leqslant L$) is mapped with ($N - M$) nodes. The Mth node coinciding always with the position of the interface, the nodal points move with time and the two grids in the α and γ regions have variable mesh sizes. In order to solve the diffusion equations in both phases, the variable domains $x \in [0;s(t)]$ and $x \in [s(t);L]$ are transformed into fixed domains $\epsilon \in [0;1]$ and $\delta \in [0;1]$:

$$\epsilon = \frac{x}{s(t)}$$

and

$$\delta = \frac{x - s(t)}{L - s(t)}. \tag{A1}$$

In the α phase the concentration field $c_\alpha(x, t)$ is transformed into $c_\alpha[x(\epsilon, t), t]$ and the following new partial derivatives can be introduced:

$$\left[\frac{\partial c_\alpha}{\partial x}\right]_t = \left[\frac{\partial c_\alpha}{\partial \epsilon}\right]_t \cdot \left[\frac{\partial \epsilon}{\partial x}\right]_t = \frac{1}{s(t)}\left[\frac{\partial c_\alpha}{\partial \epsilon}\right]_t \tag{A2}$$

$$\left[\frac{\partial c_\alpha}{\partial t}\right]_x = \left[\frac{\partial c_\alpha}{\partial t}\right]_\epsilon + \left[\frac{\partial c_\alpha}{\partial x}\right]_t \cdot \left[\frac{\partial x}{\partial t}\right]_\epsilon = \left[\frac{\partial c_\alpha}{\partial t}\right]_\epsilon + \frac{\epsilon}{s}\frac{\mathrm{d}s}{\mathrm{d}t}\left[\frac{\partial c_\alpha}{\partial \epsilon}\right]_t \tag{A3}$$

Introducing equations (A2) and (A3) into equation (5) gives for the α phase:

$$\frac{\partial c_\alpha}{\partial t} = \frac{\epsilon}{s} v \frac{\partial c_\alpha}{\partial \epsilon} + \frac{m}{\epsilon s^2} D_\alpha \frac{\partial c_\alpha}{\partial \epsilon} + \frac{1}{s^2}\frac{\partial}{\partial \epsilon}\left[D_\alpha \frac{\partial c_\alpha}{\partial \epsilon}\right] \tag{A4}$$

where the velocity of the interface $v = \mathrm{d}s/\mathrm{d}t$ has been used. A similar equation is derived for the γ phase:

$$\frac{\partial c_\gamma}{\partial t} = \frac{1 - \delta}{L - s} v \frac{\partial c_\gamma}{\partial \delta} + \frac{mD_\gamma}{[(L - s)\delta + s](L - s)} \frac{\partial c_\gamma}{\partial \delta} + \frac{1}{(L - s)^2}\frac{\partial}{\partial \delta}\left[D_\gamma \frac{\partial c_\gamma}{\partial \delta}\right]. \tag{A5}$$

Introduce a variable A_i^j representing the average diffusion coefficient at time step j for the mesh located between nodes i and $i - 1$. It is calculated using the following relationship:

$$A_i^j = \frac{D_i^j + D_{i-1}^j}{2}, \tag{A6}$$

where $D_i^j = D_v(c_i^j, T_j)$ is the diffusion coefficient at node i and time step j estimated according to the nodal concentration c_i^j, the temperature T_j and the phase v.

Using the variables (ϵ, t) and (γ, t) for the domains Ω_α and Ω_γ, an implicit discretization of the solute conservation equations gives the following relationships for the various nodes.

Nodes i with $2 \leqslant i \leqslant M - 2$ (phase α, equation (A4)):

$$\frac{c_i^j - c_i^{j-1}}{\Delta t} = \left[\frac{\epsilon_i}{s} v + \frac{m \cdot D_i^{j-1}}{\epsilon_i s^2}\right]\frac{c_{i+1}^j - c_{i-1}^j}{2\Delta\epsilon} + \frac{1}{s^2\Delta\epsilon}\left[A_{i+1}^{j-1}\frac{c_{i+1}^j - c_i^j}{\Delta\epsilon} - A_i^{j-1}\frac{c_i^j - c_{i-1}^j}{\Delta\epsilon}\right]. \tag{A7}$$

Nodes i with $M + 1 \leqslant i \leqslant N - 1$ (phase γ, equation (A5)):

$$\frac{c_i^j - c_i^{j-1}}{\Delta t} = \left[\frac{1 - \delta_i}{L - s} v + \frac{m \cdot D_i^{j-1}}{(L - s)[(L - s)\cdot\delta_i + s]}\right]\frac{c_{i+1}^j - c_{i-1}^j}{2\Delta\delta} + \frac{1}{(L - s)^2\Delta\delta}\left[A_{i+1}^{j-1}\frac{c_{i+1}^j - c_i^j}{\Delta\delta} - A_i^{j-1}\frac{c_i^j - c_{i-1}^j}{\Delta\delta}\right]. \tag{A8}$$

Node M (α/γ interface condition, equation (6))

$$v(k - 1)c_M^j = \frac{A_{M+1}^{j-1}}{L - s}\frac{c_{M+1}^j - c_M^j}{\Delta\delta} - \frac{A_M^{j-1}}{s}\frac{k\,c_M^j - c_{M-1}^j}{\Delta\epsilon} \tag{A9}$$

Notice that the concentration c_M^j refers to the concentration c_γ^* at the interface in the γ phase, the concentration c_α^* being given by $(k\,c_M^j)$, where k is the partition coefficient (i.e. $k = c_\alpha^*/c_\gamma^*$).

Node $M - 1$:

$$\frac{c_{M-1}^j - c_{M-1}^{j-1}}{\Delta t} = \left[\frac{\epsilon_{M-1}}{s} v + \frac{m}{\epsilon_{M-1}\cdot s^2} D_{M-1}^{j-1}\right]\frac{k\,c_M^j - c_{M-2}^j}{2\Delta\epsilon}$$

$$+\frac{1}{s^2\Delta\epsilon}\left[A_M^{i-1}k\frac{c_M^i-c_{M-1}^i}{\Delta c}-A_{M-1}^{i-1}\frac{c_{M-1}^i-c_{M-2}^i}{\Delta\epsilon}\right] \quad \text{(A10)}$$

Node 1 (closed system):

$$\frac{c_1^i-c_1^{i-1}}{\Delta t}=\frac{2A_2^{i-1}}{s^2\Delta c^2}(c_2^i-c_1^i) \quad \text{(A11)}$$

Node N (closed system):

$$\frac{c_N^i-c_N^{i-1}}{\Delta t}=\frac{2A_N^{i-1}}{(L-s)^2\Delta\delta^2}(c_N^i-c_{N-1}^i). \quad \text{(A12)}$$

The interface velocity v is unknown in this implicit formulation. Therefore, iterations have to be performed in order to satisfy all the equations, in particular those valid for the interface position.